

# Heralded Single-Photon Emission from the Mollow Triplet Sidebands of a Quantum Dot

A. Ulhaq\*, S. Weiler, S. M. Ulrich, R. Roßbach, M. Jetter & P. Michler

*Institut für Halbleiteroptik und Funktionelle Grenzflächen,*

*Universität Stuttgart, Allmandring 3,*

*70569 Stuttgart, Germany.*

\* *Email correspondence: ata.ulhaq@ihfg.uni-stuttgart.de*

Emission from a resonantly excited quantum emitter is a fascinating research topic within quantum optics and a useful source for different types of quantum light fields. The resonance spectrum consists of a single spectral line below saturation of a quantum emitter which develops into a triplet at powers above saturation of the emitter [1–3]. The spectral properties of the triplet strongly depends on pump power [4, 5] and detuning of the excitation laser. The three closely spaced photon channels from the resonance fluorescence have different photon statistical signatures [6]. We present a detailed photon-statistics analysis of the resonance fluorescence emission triplet from a solid state-based artificial atom, i.e. a semiconductor quantum dot. The photon correlation measurements demonstrate both 'single' and 'heralded' photon emission from the Mollow triplet sidebands [6]. The ultra-bright and narrowband emission (5.9 MHz into the first lens) can be conveniently frequency-tuned by laser detuning over 15 times its linewidth ( $\Delta\nu \approx 1.0$  GHz). These unique properties make the Mollow triplet sideband emission a valuable light source for, e.g. quantum light spectroscopy and quantum information applications [7].

Generation of non-classical light fields like single-, entangled- and heralded-photons form a vital part of many schemes of quantum information and computation. Atom optics demonstrated the heralded emission of single photons using resonance fluorescence from single atoms [8] and from cold atoms in a cavity [9]. Currently most of the heralded photon schemes use sources based on parametric down conversion [10]. Recently, there has been important developments in fiber-based heralded photon sources using four-wave mixing [11]. Both of these techniques present Poissonian statistics with photon bandwidths usually larger than 100 GHz. The increased two-photon yield in these photon sources is at the expense of fidelity. Semiconductor QDs have demonstrated single- [12], entangled- [13, 14] and heralded-photon sources [15] but mostly under non-resonant excitation schemes. Though, coherent excitation conditions of those quantum emitters are an important precondition since these promise to minimize most of the dephasing caused by the non-resonant, i.e. incoherent processes [7]. Coherent control of QD excitons has been demonstrated in a variety of experiments exhibiting Rabi splitting [16], Rabi oscillations [17], and resonant absorption [18, 19]. Observations of oscillations in the first-order correlation [20], charac-

teristic emission spectra in the frequency domain [21], and oscillations of the second-order photon correlation function [2] were all measured directly on the resonance emission from the QD. In particular, single-photon emission from a single fluorescence line (below the emitter saturation) along with photon indistinguishability as high as 90% was demonstrated [3]. Also the AC Stark shift of an exciton was used to bring the initially split QD exciton components into resonance with each other, thus forming a polarization-entangled photon source [22]. Resonant studies on solid state quantum emitters have also highlighted some of the fundamental differences vis-a-vis isolated 'real' atoms. It was particularly demonstrated that Mollow spectra at large Rabi splittings show linewidth broadening due to the presence of excitation induced dephasing (*EID*) in these quantum emitters [4, 5]. Nevertheless, pure resonant excitation appears to be the ultimate way to achieve sources of nearly Fourier transform-limited photons preferable to any non-resonant excitation scheme. Here we extend the applications of resonance excitation of a QD to demonstrate single and 'heralded' photon generation from the Mollow triplet sideband emission.

We study the case where resonant pump coherently evolves the system with 'Rabi' frequency ( $\Omega$ ) larger than the natural linewidth of the exciton transition ( $\Omega \gg \Gamma_{rad}$ ). The characteristic resonance fluorescence spectrum of such a strongly driven system consists of three distinct spectral components denoted as the 'Mollow triplet' [1]. These can be identified as the 'Rayleigh' line ( $R$ ) decorated by spectrally symmetric satellite peaks with the 'fluorescence' line ( $F$ ) as the low energy component and the 'three photon' line ( $T$ ) as the high energy sideband (for terms convention see [23]). These spectral components are a result of spontaneous emission down a ladder of pairs of so called 'dressed states'. The dressed states are a representation of the combined QD state and laser mode along with the coupling between them [24]. Each rung of the ladder (with  $N$  number of quanta) consists of two components, i.e.  $|1\rangle = c|g, N + 1\rangle + s|e, N\rangle$  and  $|2\rangle = c|g, N + 1\rangle - s|e, N\rangle$ , where  $|g, N + 1\rangle$  and  $|e, N\rangle$  represent the eigen-states of the uncoupled quantum emitter and laser states. The dressed states' components are energetically separated by the generalized Rabi frequency ( $\Omega$ ) given by the 'bare' Rabi frequency ( $\Omega_0$ ) and the laser-QD detuning ( $\Delta$ ) as  $\Omega = \sqrt{\Omega_0^2 + \Delta^2}$ . The amplitudes of the dressed eigen-states are given as  $c = \sqrt{(\Omega + \Delta)/(2\Omega)}$  and  $s = \sqrt{(\Omega - \Delta)/(2\Omega)}$ . The dressed states' eigen-energies as a function of laser detuning  $\Delta$  are plotted in Fig. 1(a).

For large positive detunings  $|\Delta| \gg 0$ , a close inspection of the steady state solution of these dressed states reveal that state  $|1\rangle$  obtains mainly  $|g, N + 1\rangle$  character and the system is mostly prepared in state  $|1\rangle$  as  $c^2 \gg s^2$  [6]. Thus a  $T$  photon is emitted first which puts the system into state  $|2\rangle$  of the next lower manifold  $E(N)$ , from where an  $F$  photon emission can finally occur (see Fig. 1(b)). This time-ordered cascaded emission of a  $T$  photon 'heralding' the  $F$  transition will result in a photon bunching signature in photon cross-correlation experiments of the Mollow sidebands which will be demonstrated below. In contrast, an autocorrelation measurement on an individual sideband should show antibunching because after emission of e.g., a  $T$  photon, emission of an  $F$  sideband photon should occur before another  $T$  photon emission is possible and vice versa (see Figs. 1(b) and (c)). In contrast, photons from the central Rayleigh line should be totally uncorrelated in time, i.e. Poissonian distributed, as the emission of an  $R$  photon is not accompanied by population modulation of the emitter's state [6].

Figure 1(d) shows a Mollow triplet series obtained at a constant excitation power under systematic variation of laser detuning  $\Delta$ . The central peak shifts along with the laser and the satellite sidebands always remain spectrally symmetric with respect to the center. As can be clearly traced in Fig. 1(e), the total Rabi splitting  $\Omega$  increases with increasing detuning  $\Delta$ . The linewidth of the Mollow sidebands in the resonant spectrum ( $\Delta = 0$ ) is found to be  $\Delta\nu = 730 \pm 20$  MHz at the corresponding Rabi frequency of  $\Omega_0 = 5.4$  GHz.

A two steps signal filtering process, initially via a Michelson interferometer [25] (see Figs. 2(a)-(c)) and secondly via a spectrometer, ensures spectral purity of the photons in Mollow triplet channels. Worth to note, an average photon count of  $70,000 \text{ s}^{-1}$  was obtained on each Mollow sideband after spectral filtering, which corresponds to a collection of 5.9 million photons per second from the sample by the objective of our confocal microscope.

Figure 2(d) shows a photon correlation measurement taken on the central Mollow peak (see also Fig. 2(c)). Remarkably, the autocorrelation demonstrates long time scale bunching instead of pure Poissonian statistics. Such an effect is commonly detected for QD recombination signal subject to 'blinking' of the excitonic state between two or more

neighboring competing states [26]. The timescale of these processes can vary from 10 ns to a few hundred ns depending on pump power [26]. The phenomenon of blinking under pure-resonant excitation can be assigned to the presence of a competing QD exciton spin configuration known as the dark excitonic state, which is non-radiative in nature [27]. Our  $g^{(2)}(\tau)$  correlation data is fitted by a bi-directional exponential fit which reveals the explicit power-dependent blinking time scale and observed in all the photon correlation measurements shown in this work.

Results of photon autocorrelation measurement taken on a spectrally separated Mollow sideband ( $T$ ) are depicted in Fig. 2(e). The whole signal is superimposed by the above-mentioned bunching-effect due to 'blinking'. The signal around zero delay exhibits clear antibunching with a normalized value of  $g^{(2)}(\tau) = 0.18$  at  $\tau = 0$ , considering the time resolution of the detection setup. From the experimental signature of antibunching, we derive a time constant of  $\tau_{fit} = 0.8 \pm 0.1$  ns, which is somewhat smaller than the theoretically expected value [6] (see supplemental material). We interpret the presence of a finite background in the correlation measurement as a consequence of signal contribution from the spectrally-close central peak of the Mollow triplet as non-vanishing background in the PL spectrum (see inset Fig. 2(e)).

Figure 3(a) demonstrates excerpts of a series of correlation measurements taken on both the sidebands simultaneously without spectral separation between them. Consequently, there is no time ordering between the sidebands photon emission as either of them can initiate a 'start' or 'stop' signal in the photon counting process. The data of Fig. 3(a) represents three distinct cases, i.e. the laser near the exact QD s-shell ( $\Delta \approx 0$ ; center), blue-detuned ( $\Delta > 0$ ; top) and red-detuned ( $\Delta < 0$ ; bottom), from the resonance. As expected a short time scale *symmetric* bunching feature is clearly observed on both the detuned cases  $\Delta \neq 0$ . The resonant case  $\Delta \approx 0$  doesn't show such bunching as the probability of both the  $F$  and  $T$  as a first photon in the cascade is equal and hence no heralded emission is expected. Again, all the three measurements reveal the long time scale ( $\Gamma_{bl}^{-1} = 42$  ns here) bunching effect corresponding to the 'blinking' of the state. Figure 3(b) displays the measured evolution of the bunching strength as a function of the detuning  $\Delta$  for two different fixed bare Rabi energies  $\Omega_0$ . A symmetric increase of the bunching

signature to either side of the detuning is observed as is obvious from the dashed lines as guide to the eye in the figure. Even though the 'heralding' nature of photon emission is observed, the time ordering is still not observed due to the simultaneous detection of both sidebands.

Figure 4(a) and (b) show cross-correlation measurements between the spectrally separated opposite sidebands of the Mollow triplet in which the  $T$  photon always act as a 'start' and the  $F$  photon as a 'stop' signal, respectively. In each case, a short time scale bunching with a time *asymmetric* peak is now observed. Fig. 4(a) shows the case of a strongly blue-detuned ( $|\Delta|/\Omega \sim 83\%$ ) laser with an abrupt rising of the bunching signal (0.48 ns, equivalent to the response time of detectors) for negative delay times and a longer exponential decay (0.94 ns) for positive delays. This directly reflects that each  $F$  photon is 'heralded' by a  $T$  photon (see Fig. 1(b)). Fig. 4(b) shows the case of a strongly red-detuned ( $|\Delta|/\Omega \sim 79\%$ ) laser where the time ordering is now reversed, i.e. here the  $T$  photon is heralded by the  $F$  photon (see Fig. 1(c)). The falling edge of the correlation functions can be perfectly fitted by the time scales ( $0.94 \pm 0.10$  ns for blue-detuned;  $0.89 \pm 0.10$  ns for red-detuned case) close to the theoretically predicted photon emission rates given by  $\Gamma = \Gamma_{rad}(c^4 + s^4)$  [6], yielding values of  $1.10 \pm 0.13$  ns (blue-detuned) and  $1.15 \pm 0.10$  ns (red-detuned), respectively.

In conclusion, we have demonstrated that an individual Mollow sideband channel of the resonance fluorescence from a single quantum dot can act as an efficient single-photon source. By spectrally separating both the Mollow sidebands, we showed that this source can act as a solid state-based heralded photon emitter as well. Possible applications of such high-brightness photon sources include the realization of semiconductor-atom interfaces for the development of photon based-memories [28]. Heralded photon sources may find applications in quantum communication protocols [29]. These high yield and narrow band sources might also be invaluable for spectroscopy of quantum emitters, where non-classical light is used for the excitation process. Using the Purcell effect by embedding the QDs in optical microcavities can result in spectrally ultrasharp emission lines [30]. Tuning the cavity into resonance with one of the Mollow triplet sideband can result in population inversion of the system and ultimately single quantum emitter lasing [31].

## Method Summary

The sample consist of a single layer of self-assembled In(Ga)As quantum dots grown by metal-organic vapor-phase epitaxy (MOVPE). The quantum dot layer is sandwiched between GaAs/AlAs DBR layers at the center of a GaAs  $\lambda$ -cavity. The sample is kept in a Helium-flow cryostat which is capable to stabilize the temperature to  $5 \pm 0.5$  K. The measurements are performed on a special micro-Photoluminescence ( $\mu$ PL) setup [3] with orthogonal geometry between the laser excitation in the growth plane, in combination with detection of luminescence perpendicular to the sample surface. The DBR structure of the sample acts as a waveguide for the excitation laser. Additional to  $90^\circ$  geometry, a pinhole assembly is employed to minimize the contribution of scattered laser light. A polarizer setup containing a high-extinction Glan Thompson polarizer further suppresses the collection of laser stray light via polarization selection. An individual QD is addressed by a narrow-band ( $\sim 500$  kHz) cw Ti:Sa laser by tuning it into the s-shell of a QD. While scanning the narrowband laser over the QD s-shell resonance, enhancement of the signal is an indication of the onset of resonance fluorescence. The spectrometer + CCD combination in the setup has a resolution of 8.4 GHz, which cannot resolve the components of Mollow emission spectrum particularly at lower excitation powers. To obtain a detailed spectrum of the full Mollow triplet, with well-resolved sidebands, we use a scanning Fabry-Pérot interferometer providing a resolution of less than  $\sim 250$  MHz.

In order to perform correlation measurements on different spectral components of the Mollow triplet, it is important to have an efficient filtering mechanism. For this purpose, a Michelson interferometer is employed for pre-filtering. The delay of the interferometer is kept in such a way that the photons from Mollow sidebands interfere constructively on one output, while the central Mollow peak leave the other output of the interferometer. After the spatial separation of the sidebands and the central peak, further filtering is performed via two spectrometers with spectral resolutions of 8.4 and 9.6 GHz, respectively. The same spectral component of the Mollow emission spectrum is selected to perform photon auto-correlation, while for cross-correlations different components are selected by each spectrometer.

- 
- [1] Mollow, B. R. Power Spectrum of Light Scattered by Two-Level Systems. *Phys. Rev.* **188**, 1969 (1969).
- [2] Flagg, E. B., *et al.* Resonantly driven coherent oscillations in a solid-state quantum emitter. *Nature Physics* **5**, 203-207 (2009).
- [3] Ates, S., *et al.* Post-Selected Indistinguishable Photons from the Resonance Fluorescence of a Single Quantum Dot in a Microcavity. *Phys. Rev. Lett.* **103**, 167402 (2009).
- [4] Ulrich, S. M., *et al.* Dephasing of Mollow Triplet Sideband Emission of a Resonantly Driven Quantum Dot in a Microcavity. *Phys. Rev. Lett.* **106**, 247403 (2011).
- [5] Roy, C. & Hughes, S. Phonon-dressed Mollow triplet in the regime of cavity-QED. *Phys. Rev. Lett.* **106**, 247402 (2011).
- [6] Schrama, A., Nienhuis, G., Dijkerman, H. A., Steijsiger, C. & Heideman, H. G. Intensity correlations between the components of the resonance fluorescence triplet. *Phys. Rev. A* **45**, 8045 (1992).
- [7] Kiraz, A., Atatüre, M. & Imamoglu. Quantum-dot single-photon sources: Prospects for applications in linear optics quantum-information processing. *Phys. Rev. A* **69**, 032305 (2004).
- [8] Aspect, A., Roger, G., Reynaud, S., Dalibard, J. & Cohen-Tannoudji, C. Time Correlations between the Two Sidebands of the Resonance Fluorescence Triplet. *Phys. Rev. Lett.* **45**, 617-620 (1980).
- [9] Thompson, J. K., Simon, J., Huanquian, L. & Vuletić, V. A High-Brightness Source of Narrowband, Identical-Photon Pairs. *Science* **313**, 74-77 (2006).
- [10] Fasel, S., *et al.* High-quality single asynchronous heralded single-photon source at telecom wavelength. *N. J. Phys.* **6**, 163 (2004).
- [11] Cohin, O., *et al.* Tailored Photon-Pair Generation in Optical Fibers. *Phys. Rev. Lett.* **102**, 123603 (2009).
- [12] Michler, P., *et al.* A Quantum Dot Single-Photon Turnstile Device. *Science* **290**, 2282-2285 (2000).
- [13] Akopian, N., *et al.* Entangled Photon Pairs from Semiconductor Quantum Dots. *Phys. Rev. Lett.* **96**, 130501 (2006).



- [14] Stevenson, R. M., *et al.* A semiconductor source of triggered entangled photon pairs. *Nature* **439**, 179-182 (2006).
- [15] Moreau, E., *et al.* Quantum Cascade of Photons in Semiconductor Quantum Dots. *Phys. Rev. Lett.* **87**, 183601 (2001).
- [16] Kamada H, *et al.* Exciton Rabi oscillation in a single quantum dot. *Phys. Rev. Lett.* **87**, 246401 (2001).
- [17] Zrenner, A., *et al.* Coherent properties of a two-level system based on a quantum-dot photodiode. *Nature* **418**, 612-614 (2002).
- [18] Xu, X., *et al.* Coherent Optical Spectroscopy of a Strongly Driven Quantum Dot. *Science* **317**, 929-932 (2007).
- [19] Jundt, G., *et al.* Robledo, L., Högele, A., Fält, S. & Imamoglu, A. Observation of Dressed Excitonic States in a Single Quantum Dot. *Phys. Rev. Lett.* **100**, 177401 (2008).
- [20] Muller, A., *et al.* Resonance Fluorescence from a Coherently Driven Semiconductor Quantum Dot in a Cavity. *Phys. Rev. Lett.* **99**, 187402 (2007).
- [21] Vamivakas, A. N., Zhong, Y., Yong, C.-Y. & Atature, M. Spin-resolved quantum-dot resonance fluorescence. *Nature Physics* **5**, 198-202 (2009).
- [22] Muller, A., Fang, W., Lawall, J. & Solomon, G. S. Creating Polarization-Entangled Photon Pairs from a Semiconductor Quantum Dot Using the Optical Stark Effect. *Phys. Rev. Lett.* **103**, 217402 (2009).
- [23] Nienhuis, G. Spectral correlations in resonance fluorescence. *Phys. Rev. A* **47**, 510-518 (1993).
- [24] Cohen-Tannoudji, C., Dupont-Roc, J. & Grynberg, G. *Atom-Photon Interactions* (Wiley-VCH Weinheim, 2004).
- [25] Aichele, T., Reinaudi, G. & Benson, O. Separating cascaded photons from a single quantum dot: Demonstration of multiplexed quantum cryptography. *Phys. Rev. B* **70**, 235329 (2004).
- [26] Santori, C., Pelton, M., Salamo, G., Dale, Y. & Yamamoto, Y. Triggered Single Photons from a Quantum Dot. *Phys. Rev. Lett.* **86**, 1502 (2001).
- [27] Bayer, M., *et al.* Fine structure of neutral and charged excitons in self-assembled In(Ga)As/(Al)GaAs quantum dots. *Phys. Rev. B* **65**, 195315 (2002).
- [28] Akopian, N., Wang, L., Rastelli, A., Schmidt O. G & Zwiller, V. Hybrid semiconductor-atomic interface: slowing down single photons from a quantum dot. *Nat. Phot.* **5**, 230-233 (2011).
- [29] Gisin, N. & Thew, R. Quantum Communication. *Nat. Phot.* **1**, 165-171 (2007).

- [30] Freedhoff, H. & Quang, T. Ultrasharp Lines in the Absorption and Fluorescence Spectra of an Atom in a Cavity. *Phys. Rev. Lett.* **72**, 474 (1994).
- [31] Quang, T. & Freedhoff, H. Atomic population inversion and enhancement of resonance fluorescence in a cavity. *Phys. Rev. A.* **47**, 2285 (1993).

### **Acknowledgements**

The authors greatly acknowledge D. Richter and W.-M. Schulz for providing high quality sample, and M. Wiesner for help in sample processing. The authors gratefully acknowledge financial support by the DFG research group 730. A. Ulhaq acknowledges funding from International Max Planck Research School IMPRS-AM. S. Weiler acknowledges financial support by the Carl-Zeiss-Stiftung.

### **Author contributions**

R.R. and M.J. designed the sample structure. A.U., S.W., S.M.U. and P.M. conceived the experiments. A.U., S.W. and S.M.U. performed the experiments and analyzed the data. A.U., S.W., S.M.U. and P.M. wrote the article, with input from the other co-authors.

**Figure 1: Laser-detuning dependent Mollow triplet spectra.** (a) Laser-QD-detuning dependence of dressed state eigen-energies (solid lines), together with the QD + laser uncoupled eigenstates (dashed lines) [24]. (b) and (c) Sideband photon emission sequence down the dressed states ladder for a strong blue-detuned ( $\Delta \gg 0$ , (b)) and a red-detuned ( $\Delta \ll 0$ , (c)) laser case. (d) Laser detuning-dependent resonance fluorescence spectra recorded in high-resolution PL. All the spectra are taken at the same excitation power of  $P = 500 \mu\text{W}$ . (e) Positions of the spectral components of the fluorescence signal derived from the detuning series in (d). Solid lines are fits according to  $\nu = \Delta \pm \sqrt{\Omega_0^2 + \Delta^2}$  and  $\nu = \Delta$ .

**Figure 2: Photon correlations on Mollow spectral components.** (a) Michelson interferometer setup used to spatially separate the Mollow sidebands from the central line (see supplementary information). (b) Mollow spectrum obtained after filtering out the central peak, where only the sidebands remain observable in high-resolution PL. (c) High-resolution spectrum of the central Rayleigh line filtered from the Mollow sidebands in (b). (d) Photon autocorrelation of the central Mollow triplet peak. The 'bare' Rabi frequency is 11.27 GHz while the laser is at exact resonance with the QD exciton ( $\Delta = 0$ ). The solid line is a bi-directional exponential fit to the data to extract the effect of 'blinking'. Inset: PL spectrum of the full Mollow triplet obtained with the shaded region as the selected spectral region for photon correlation measurement. (e) Auto-correlation on the  $T$  line of the Mollow spectrum. The experimental conditions were  $\Omega_0 = 11.27$  GHz and  $\Delta = 0$ . The solid red (blue dashed) line is a theoretical fit of the signal, convoluted (deconvoluted) with the instrumental detector response (480 ps). Inset: PL spectrum after filtering out the central line. The shaded region shows the spectrally selected signal for the autocorrelation measurement.

**Figure 3: Laser detuning-dependent correlation of the combined Mollow sidebands signal.** (a) Photon correlation measurement on both Mollow triplet sidebands, without any time-ordering. The measurements are performed on resonance with the QD s-shell (center), blue detuned (top) and red-detuned (bottom). Inset: Corresponding PL spectrum with highlighted area as the spectrally selected signal. (b) Bunching parameter, derived from correlation measurements (a), as a function of laser-QD detuning  $\Delta$ . The data points are plotted for two different excitation powers: red ( $170 \mu\text{W}$  with  $\Omega_0 = 3.4 \text{ GHz}$ ) and black ( $500 \mu\text{W}$  with  $\Omega_0 = 5.4 \text{ GHz}$ ). Dashed lines are guides to the eye.

**Figure 4: Cross-correlation between spectrally selected Mollow sidebands.** (a) Photon correlation between the  $T$  photon ('start') and  $F$  photon ('stop') lines, where the central Rayleigh line is interferometrically suppressed. The 'bare' Rabi frequency is  $\Omega_0 = 11.1 \text{ GHz}$ , while the laser is blue-detuned by  $\Delta = +9.3 \text{ GHz}$  from exact resonance. The solid line is a theoretical fit to the data with the exponential for negative (positive) delay indicating the rising (falling) edge of the correlation signal. For this case, the steady state population of  $|1\rangle$  is 95%. (b) Same as (a) but for a case where  $\Omega_0 = 9.6 \text{ GHz}$  while  $\Delta = -7.6 \text{ GHz}$ . The rise and falling edge are time-reversed in this case. The steady state population of state  $|2\rangle$  is 95% in this case.

Figure 1

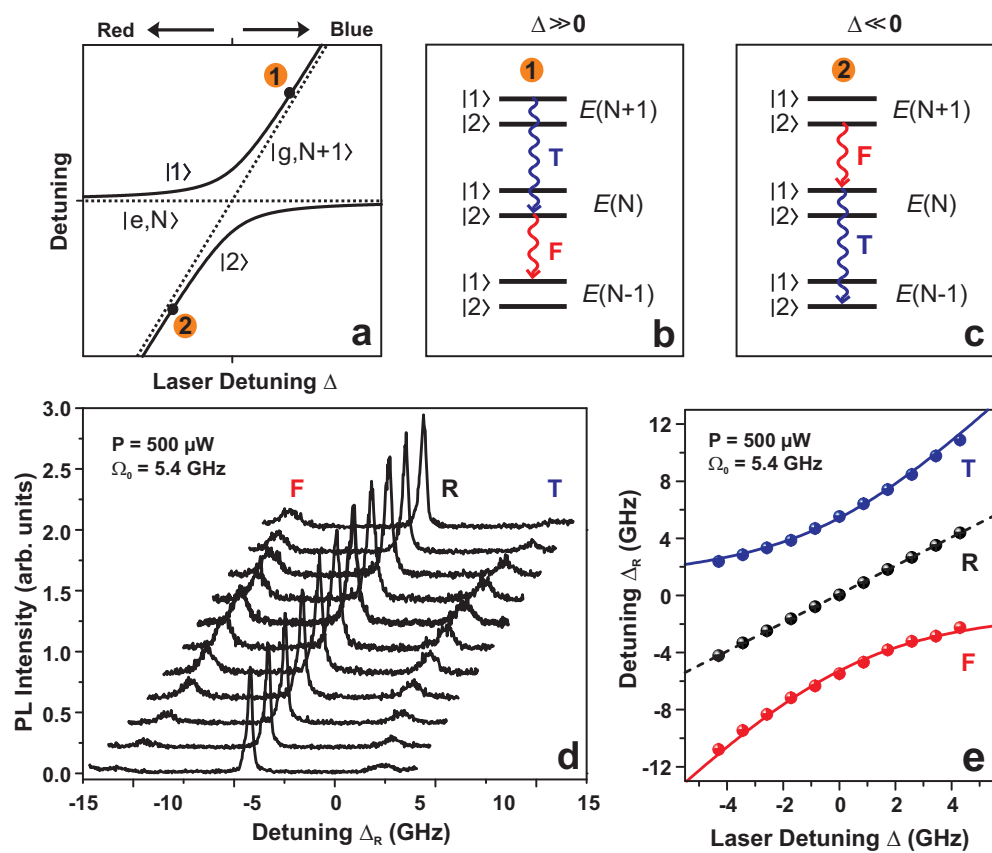


Figure 2

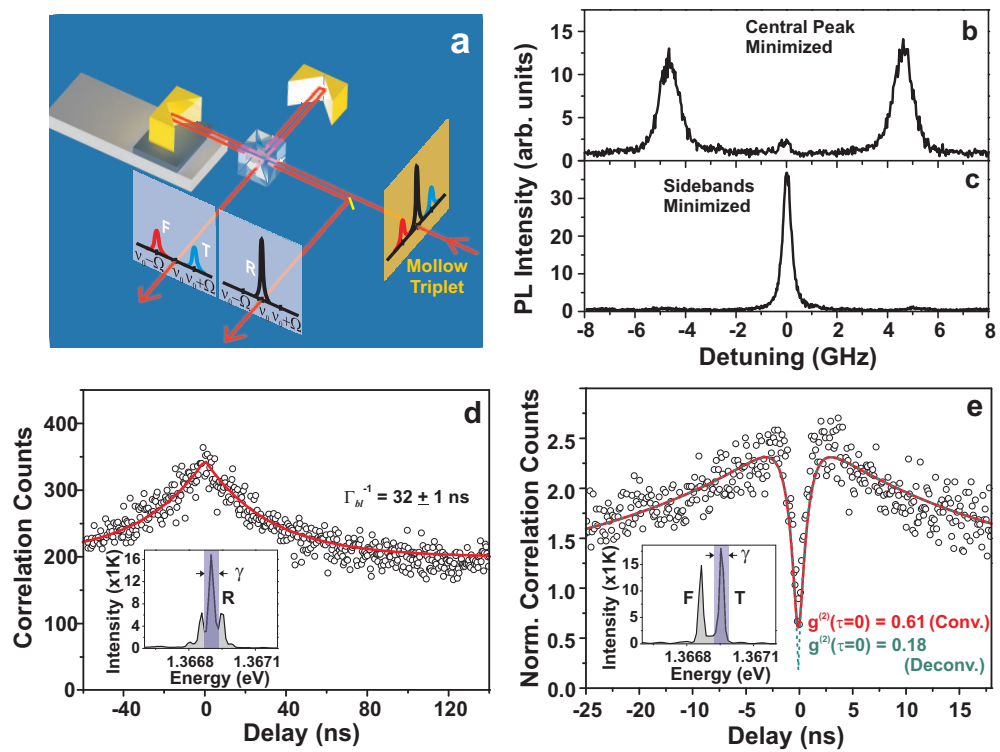


Figure 3

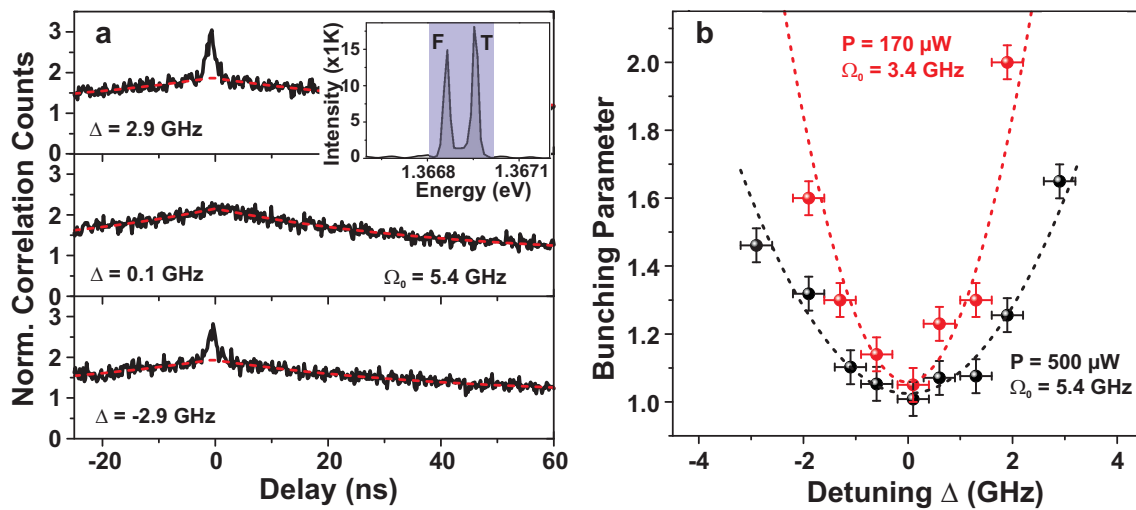
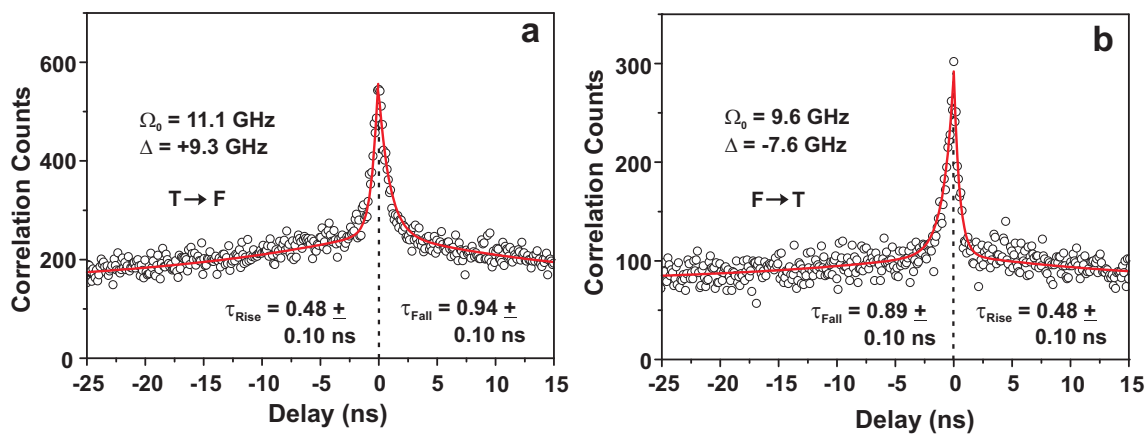


Figure 4





## Supplementary Data

In the supplementary data we provide further explanation of experimental methods and conditions. Some of the analysis has been explained and additional results are added, which give deeper insight of the concepts in the main text.

### 1. Methods

The Michelson interferometer shown in Fig. 2(a) is used to selectively suppress the sidebands or the central line of the Mollow triplet. As explained in the main text for the measurements presented in Figs. 2 (d) and (e), the sidebands or the central peak are suppressed, respectively. The probability of photons of a certain wavelength  $\lambda$  to leave one output of the interferometer beam splitter is given by [1]:

$$p(\lambda) = 0.5 + 0.5 * \cos(2\pi d/\lambda) \tag{1}$$

where  $d$  is the path length difference between the two arms of the interferometer. The path difference should be well below the coherence length of the emission. The minimum path difference for which the two components with spectral separation of  $\Delta\lambda$  are spatially separated is given by  $d_0 = \lambda(\lambda + \Delta\lambda)/(2\Delta\lambda)$ . Figure S1 plots the photon output probability of all the three components of the Mollow triplet for a Rabi splitting of 10 GHz ( $\Delta\lambda = 0.027$  nm) around  $d_0 = 15.4947$  mm (vertical black dashed line). The sideband photons (red solid and blue dashed lines) interfere constructively at  $d_0$ , while the central peak photons (black line) interferes destructively at the same output of the beam splitter. It can be readily observed that at the specific path difference (vertical dashed line) the output beam consists mainly of the sidebands and almost negligible contribution from the central peak. In contrast, the other output of the interferometer will mainly consists of the central Mollow peak. A motorized stage with a linear step resolution of 100 nm is used to accurately adjust the output of the Michelson interferometer.

For the demonstration of cross-correlation between the two sidebands, it is important that the time ordering of the heralded photon pairs is maintained by the photon detection process as well. A spectral filter of bandwidth  $\gamma$  introduces a time uncertainty of  $1/\gamma$  in the filtered photons. Thus the time ordering of the detection of each spectral component

will be maintained only if the photon arrival-time-difference  $\tau$  is larger than the inverse bandwidth ( $\gamma^{-1}$ ) of the filter (110 ps  $\leftrightarrow$  35  $\mu$ eV) [2]. The timescale between the sideband photons is given by the modified lifetime ( $\Gamma^{-1}$ ) which is greater  $\gamma^{-1}$  for the experimental data shown in Fig. 4(d) and (e) of the main text. It's noteworthy that this formulation is valid as long as the inequality  $\Omega \gg \gamma \gg \Gamma_{rad}$  is satisfied.

## 2. Data Analysis

There are two kinds of bunching effects in Figures 3 and 4, where one is a long time scale effect due to the blinking of the QD dark state as explained in the main text. These are normally longer than 10 ns. The other bunching is due to the heralded photon emission and appears on a much shorter timescale of the modified emission lifetime ( $\Gamma^{-1}$ ) of the QD exciton. The theoretical fit to these data plots are given by:

$$g^{(2)}(\tau) = 1 + c_1^2 e^{-\Gamma\tau} + c_2^2 e^{-\Gamma_{bl}\tau} \quad (2)$$

The timescale of the blinking effect has a clear pump power dependence such that its time scale decreases with increasing excitation power [3].

As mentioned in the main text, the modified emission rate  $\Gamma$  for the heralded emission from the Mollow sidebands under explicit laser-QD detuning  $\Delta$  is calculated by the relation:

$$\Gamma = \Gamma_{rad}(c^4 + s^4). \quad (3)$$

For the auto-correlation measurement in Fig. 2(e), the following parameters are expected for the conditions of zero detuning  $\Delta = 0$ :  $c^2 = 0.5$ ,  $s^2 = 0.5$ , and  $\Gamma = 1.6 \pm 0.1$  GHz.

For the experimental conditions in Figs. 4(a) and (b), the following parameters are derived: Blue-detuned case (Fig. 4(a)):  $c^2 = 0.82 \pm 0.04$ ;  $s^2 = 0.18 \pm 0.04$ ;  $\Gamma_{rad} = 1.25 \pm 0.08$  GHz,  $\Gamma = 1.13 \pm 0.10$  GHz.

Red-detuned case (Fig. 4(b)):  $c^2 = 0.19 \pm 0.04$ ;  $s^2 = 0.81 \pm 0.04$ ;  $\Gamma_{rad} = 1.25 \pm 0.08$  GHz,  $\Gamma = 1.15 \pm 0.10$  GHz.

### 3. Additional measurements (p-shell excitation)

For these measurements the QD was selectively pumped via an excited state (p-shell). The PL spectrum under these conditions show a clear exciton line from the QD (see inset of Fig. S2(a)). Figure S2(a) depicts the time correlated single photon counting (TCSPC) data from the QD. The measurement was performed through a fast response APD (response time of  $\sim 45$  ps). The data is fitted to a single exponential and yields a radiative lifetime of  $800 \pm 10$  ps of the QD exciton. Figure S2 (b) presents an auto-correlation measurement on the QD emission signal. The correlation measurement under p-shell excitation also exhibits the long time scale ( $\sim 49$  ns) 'blinking' effect resulting in a bunching of the overall data. The data points near zero delay demonstrate clear antibunching on a fast time scale (on the order of radiative emission lifetime), clearly revealing the single photon nature of the QD line. The deconvoluted fit to the data points yields an antibunching value of 0.23. The finite background can be due to a spectrally close line from another QD (see inset of Fig. S2(a)). The data has been fitted using the following theoretical function:

$$g^{(2)}(\tau) = 1 - c_1^2 e^{-\Gamma_{rad}\tau} + c_2^2 e^{-\Gamma_{bl}\tau} \quad (4)$$

where  $\Gamma_{rad}^{-1}$  is the spontaneous emission lifetime and  $\Gamma_{bl}^{-1}$  is the extracted timescale associated with the 'blinking' effect of the QD. The coefficients  $c_1$  and  $c_2$  represents the signal to noise ratio of the detected signal. The same kind of fit is used for data in Fig 2(e) of the main text.

- 
- [1] Aichele, T. *Detection and Generation of Non-Classical Light States from Single Quantum Emitters (PhD thesis)* (Logos, 2005).
  - [2] Nienhuis, G. *Phys. Rev. A* **47**, 510-518 (1993).
  - [3] Santori, C., *et al.* *Phys. Rev. Lett.* **86**, 1502 (2001).

**Figure S1: Michelson interferometer-based frequency filtering.** The probability of emission of photons at an output of the interferometer as a function of varying path difference between the two arms of the interferometer. The black solid line is the probability of the Mollow central line while the red line is the probability of the red-sideband and blue dashed line is the probability of blue sideband of the Mollow triplet. The blue line has been shifted vertically for better observation. The central line is taken at 907 nm (330531.9 GHz) while a Rabi splitting of 10 GHz is assumed.

**Figure S2: Time-resolved and photon correlation measurement under quasi-resonant excitation.** (a) Inset shows the spectrum of the QD under p-shell excitation. The data shows a time correlated photon counts from the QD line under pulsed p-shell excitation. A single exponential fit extracts the emission lifetime of the QD. (b) Autocorrelation measurement on the QD signal under quasi-resonant excitation. The solid red (dashed blue) line is a theoretical fit to the data convoluted (deconvoluted) with the instrument response function.

Figure S1

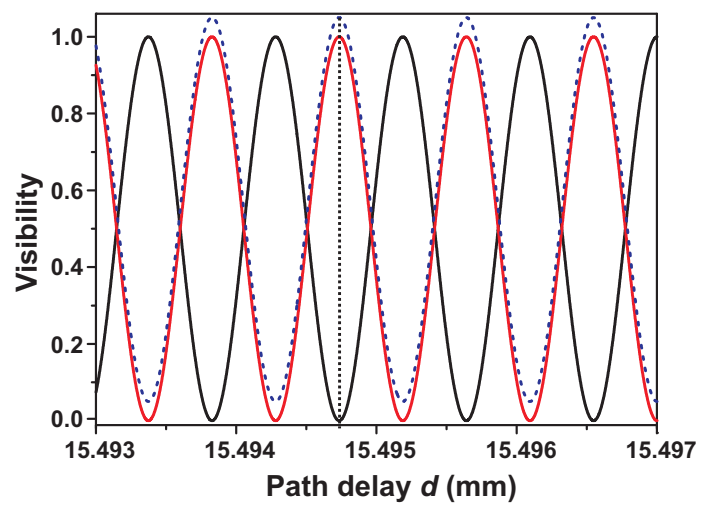


Figure S2

